Coastal cliff ground motions from local ocean swell and infragravity waves in southern California

Adam P. Young,[1] Peter N. Adams,[2] William C. O'Reilly,[1] Reinhard E. Flick,[1] and R. T. Guza[1]

Received 28 March 2011; revised 27 June 2011; accepted 11 July 2011; published 9 September 2011.

[1] Ground motions atop a southern California, USA coastal cliff are compared with water level fluctuations observed at the cliff base, and with ground motions observed 10 km inland. At high tide, cliff top ground motions in three frequency bands were generated locally by ocean waves at the cliff base: (1) high-frequency (>0.3 Hz) "shaking" caused by waves impacting the cliff, and (2) gravitational loading-induced "swaying" at the frequency of the incident sea swell waves (0.05–0.1 Hz), and (3) slow "swaying" at infragravity frequencies (0.006–0.05 Hz). At high tide, at infragravity and incident sea swell wave frequencies, cliff top vertical ground displacement and cliff base water level fluctuations are coherent and oscillate in phase (with occasional deviation at sea swell frequencies), and spectral levels at the cliff top are much higher than at the inland seismometer. In contrast, at "double frequencies" (0.1–0.3 Hz) spectral levels of vertical motions are nearly identical inland and at the cliff top, consistent with a common (distant or spatially distributed) source. At low tide, when ocean waves did not reach the cliff base, power levels of vertical ground motions at the cliff top decreased to inland levels at incident wave frequencies and higher, and only infragravity-band motions were noticeably forced by local ocean waves.

Citation: Young, A. P., P. N. Adams, W. C. O'Reilly, R. E. Flick, and R. T. Guza (2011), Coastal cliff ground motions from local ocean swell and infragravity waves in southern California, *J. Geophys. Res.*, *116*, C09007, doi:10.1029/2011JC007175.

1. Introduction

[2] Ocean wave pressure fluctuations on the seafloor drive ground motions at frequencies of the incoming sea swell (0.05–0.1 Hz, "single-frequency"), at twice the sea swell frequency ("double-frequency"), and at lower infragravity frequencies (here 0.006–0.05 Hz) [e.g., *Longuet-Higgins*, 1950; *Haubrich et al.*, 1963; *Haubrich and McCamy*, 1969; *Kibblewhite and Wu*, 1991; *Webb*, 2007]. The seafloor ground motions couple into seismic waves that propagate long distances. Shorter period ground shaking from wave impacts [*Adams et al.*, 2002], and longer period coastal ground translation and/or tilt from gravitational loading of ocean tides [*Farrell*, 1972; *Agnew*, 1997] and tsunamis [*Yuan et al.*, 2005] are also observed. Ocean-related ground motions over a wide frequency band have been recorded on the deep ocean bottom [e.g., *Dolenc et al.*, 2005, 2007], shallow-water ocean bottom [e.g., *Webb and Crawford*, 2010], at the coast [e.g., *Agnew and Berger*, 1978], and at large distances inland [e.g., *Bromirski*, 2001].

[3] Considered noise in many seismic studies, ocean-generated ground motions are useful in studies of wave hindcasting [*Tillotson and Komar*, 1997; *Bromirski et al.*, 1999], ice shelf processes [*MacAyeal et al.*, 2006, 2009; *Cathles et al.*, 2009; *Bromirski et al.*, 2010], tsunamis [*Yuan et al.*, 2005], Earth hum [*Rhie and Romanowicz*, 2004, 2006; *Webb*, 2007; *Dolenc et al.*, 2008], crustal structure [*Crawford et al.*, 1991], and coastal cliff geomorphology [*Adams et al.*, 2002, 2005]. Observations of ocean-generated seismic waves at their origin are rare, and their generation and transmission mechanics are not well understood. Here observations of seismic and ocean waves at a southern California coastal cliff, and nearby inland seismic data, are used to explore locally and nonlocally ocean-generated cliff ground motion for various frequency bands.

2. Background

[4] Coastal cliff top residents often report ground shaking by storm waves, but quantitative observations are relatively scarce. *Adams et al.* [2002] showed that the high-frequency (1–25 Hz) wave-induced cliff shaking at a central California cliff, fronted by a gently sloping submerged shore platform, depended on offshore wave conditions, shelf bathymetry, and tides. *Adams et al.* [2005] showed that high-frequency shaking from wave impacts is accompanied by cliff "sway" at the incoming sea swell frequency. Cliff sway is downward and seaward as waves approach the cliff, and decreases in ampli-

[1]Integrative Oceanography Division, Scripps Institution of Oceanography, University of California San Diego, La Jolla, California, USA.
[2]Department of Geological Sciences, University of Florida, Gainesville, Florida, USA.

0148-0227/11/2011JC007175

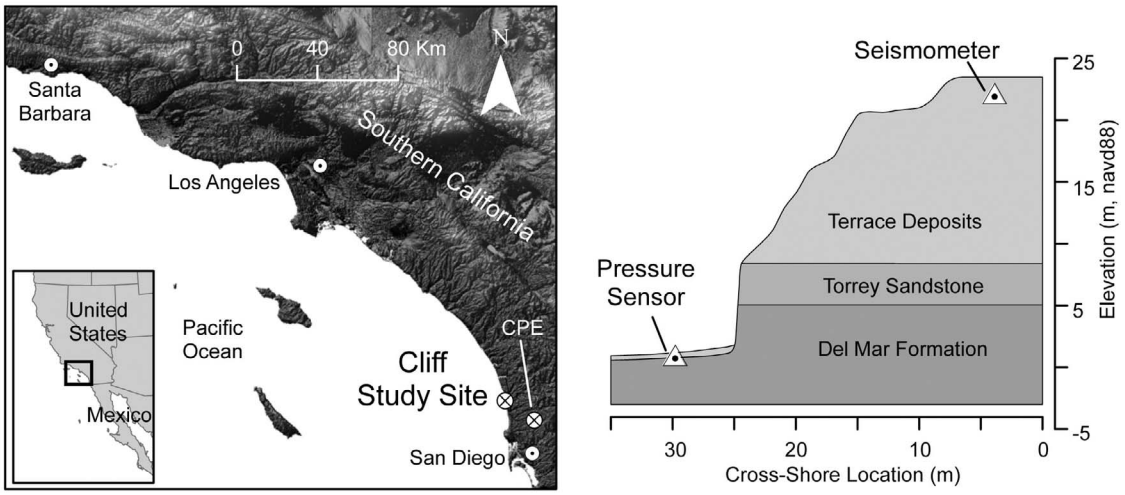

Figure 1. (left) Southern California study site location and (right) general cliff profile and instrument locations.

tude inland from the cliff edge. *Adams et al.* [2005] suggest that cyclic flexing at sea-swell frequencies may reduce the material strength of coastal cliffs through strain induced fatigue.

[5] *Pentney* [2010] observed ground motion in the 0.125–100 Hz range at the top and base of a New Zealand cliff fronted by an elevated shore platform. Similar to previous studies, cliff top ground motions increased with increasing incident wave height, decreased with distance inland, and were tidally modulated. However, in contrast with *Adams et al.* [2002, 2005], *Pentney* [2010] found that, during large-wave events, cliff top ground motion was lowest at high tide and greatest at mid-low tide, suggesting the cliff top motion was enhanced by wave energy dissipated at the seaward edge of the elevated shore platform. Dissimilar ground motions at the cliff base and top suggested that the cliff structure influenced ground response.

[6] Recently, *Lim et al.* [2011] investigated microseismic "events" associated with wave impacts at a cliff in North Yorkshire, United Kingdom, fronted by an extensive shore platform with varying structure. Distinct water elevations were associated with an elevated cliff response, suggesting a local topographic (for example, platform morphology) and/or structural influence similar to *Pentney* [2010]. Wind direction was also found to correspond with the seismic cliff response. Cliff erosion during the study period suggested a possible lag time or threshold response when compared with elevated numbers of seismic events, but more research is needed. Other seismic studies of coastal cliffs [*Amitrano et al.*, 2005; *Senfaute et al.*, 2009] primarily focused on non-ocean-related signals including high-frequency (40 Hz–10 kHz) seismic precursory patterns of cliff cracking and failures. The present study provides the first observations of cliff motion at infragravity frequencies. Additionally, cliff ground motions are compared with in situ measurements of cliff base water levels, and with a seismometer located 10 km inland.

3. Study Site

3.1. Cliff Setting

[7] The studied 24 m high cliff, located in northern Del Mar, California, USA, consists of three geologic units (Figure 1). The lower unit is the Del Mar Formation, an Eocene sedimentary deposit composed of sandy clay stone interbedded with coarse-grained sandstone, overlain conformably by Torrey Sandstone, a massive coarse-grained and well-cemented Eocene sandstone [*Kennedy*, 1975]. Together, these two units form the lower near-vertical portion of the cliff, while the upper-cliff section sloping at 35–50° consists of weakly cemented, fine-grained sandy Pleistocene terrace deposits. The contact between the Del Mar and Torrey Sandstone Formations decreases in elevation toward the north and terminates abruptly at a fault immediately north of the instrumentation setup. The cliff is fronted by a narrow sand (and occasionally cobble) beach, which is often flooded during high tides. The underlying shore platform is gently sloping and relatively smooth near the shoreline, but becomes somewhat irregular offshore, forming several near-shore reef structures.

3.2. Oceanographic Setting

[8] The cliffs are exposed to waves generated by local winds and distant storms in both hemispheres. During winter, swell from the North Pacific and Gulf of Alaska is most energetic, whereas swell from the South Pacific dominates in summer. Waves reaching southern California cliffs undergo a complex transformation, and "shadows" of the Channel Islands create strong along-shore variations in wave height [e.g., *Pawka*, 1983]. The seasonal cycle in the Del Mar region has maximum wave energy in winter. The tide range is about 2 m (http://tidesandcurrents.noaa.gov).

4. Methods

4.1. Cliff Base Water Elevations

[9] A Paroscientific pressure sensor (model 245A-102), sampling at 8 Hz from 28 January 2010 to 2 April 2010, was located on the shore platform (1.01 m, datum-NAVD88) approximately 4 m shoreward of the cliff base (Figure 1). Atmospheric pressure was removed from the record using linearly interpolated 6 min data measured about 12 km south on a pier. Pressure sensor readings were corrected for a 3 s

clock drift and converted to hydrostatic elevation relative to NAVD88.

4.2. Seismometers

[10] Ground motions were measured at 100 Hz with a Nanometrics Compact Trillium broadband velocity seismometer from 20 February 2010 to 2 April 2010 near the cliff top edge (23.5 m, NAVD88), 26 m shoreward of the pressure sensor (Figure 1). The seismometer response has −3 dB corners at 0.0083 and 108 Hz. The raw velocity data were phase and magnitude corrected in the frequency domain according to the instrument response curve for frequencies above 0.006 Hz (lower frequencies are not investigated in this study). An ANZA network seismometer (http://eqinfo.ucsd.edu/deployments/anza/index.php), located 14 km inland and 18 km southeast of the cliff site in Camp Elliot (CPE; Figure 1), was also analyzed.

[11] Broadband seismometers are sensitive to ground tilt that maps part of the vertical gravitational acceleration onto the horizontal components, resulting in apparent long-period ground motions [*Rodgers*, 1968]. Tilt effects increase with increasing period, and can contribute significantly to horizontal accelerations at infragravity frequencies [*Webb and Crawford*, 1999; *Crawford and Webb*, 2000]. Tilt effects on the vertical component are generally considered negligible [*Graizer*, 2006]. However, a small component of the longest-period vertical signals during high tides could be caused by tilt.

[12] Integration of the vertical and horizontal velocity output yields time series of vertical ground displacement, and "apparent horizontal displacement" (where the relative contributions of displacement and tilt are unknown), respectively. Cross-shore and along-shore apparent displacement time series were obtained by rotating (counterclockwise 14°) the horizontal channels (E-W and N-S) into the approximate local shoreline orientation. The cross-shore sign convention is that positive apparent displacement corresponds to onshore displacement and landward tilt.

[13] Seismic and cliff base water levels, divided into 1 h records, were processed with standard Fourier spectral and cross-spectral methods [*Jenkins and Watts*, 1968]. Hours containing significant ground motion from earthquakes, postinstallation settlement, or local noise were removed manually.

4.3. Incident (10 m Depth) Wave Height

[14] A wave buoy network (Coastal Data Information Program (CDIP), http://cdip.ucsd.edu) was used to estimate hourly significant wave height at virtual buoys or "monitored and prediction" points (MOPS) seaward of the study area in 10 m depth at 100 m intervals along-shore. The effects of complex bathymetry in the southern California Bight, and of varying beach orientation and wave exposure, were simulated with a spectral refraction wave model initialized with offshore buoy data [*O'Reilly and Guza*, 1991, 1993, 1998]. Incident significant wave height (10 m depth) was estimated as the mean of the five closest MOP locations.

5. Observations

[15] Tide level and incident wave height (Figures 2a and 2b) influenced water levels at the cliff base (Figures 2c and 2d), and ground motions at the cliff top (Figures 2e–2g). Cliff top ground displacements and cliff base wave heights were maximum in early March when energetic incident waves and spring high tides coincided. Cliff base water level fluctuations are correlated with all three components of (apparent) cliff top ground displacement (Figure 2). The cross-shore component of apparent ground displacement was consistently larger than along-shore and vertical components.

[16] Time series of cliff top ground displacement, band-passed into three broad frequency bands, (high-frequency shaking, combined single- and double-frequency incident waves, and infragravity), are shown at a typical high tide with moderate waves (31 March 2010 UTC) in Figures 3a–3c, respectively. Displacements (both apparent horizontal and vertical) are larger in the infragravity band than in the sea swell and shaking bands, and vertical displacements are smaller than apparent horizontal displacements. At the cliff base, water level fluctuations in the infragravity and incident bands are both significant and have similar amplitudes (Figures 3d and 3e). High-frequency shaking (>0.3 Hz) occurs at high tide (Figure 3a), when broken (or near breaking) sea swell wave crests directly impact the cliff, as observed previously. At low tide (not shown), waves do not reach the cliff base (the subaerial beach is usually between about 35 and 50 m wide), wave-cliff impact spikes in the shaking time series are absent, and energy levels in all bands are much reduced.

[17] At high tide, cliff base water levels are coherent with cliff top vertical ground motions in the infragravity (0.006–0.05 Hz) and single frequency (0.05–0.1 Hz) bands (Figure 4d). Cliff top ground displacements in these bands, and in the shaking band (>0.3 Hz), are usually at least several times larger than 10 km inland (Figure 4b). In contrast, the magnitudes of vertical displacements at "double-frequencies" (0.1–0.2 Hz) are nearly identical at the cliff top and inland seismometers, consistent with a common (distant or spatially distributed) source. The approximately 180° phase difference between cliff top vertical displacements and cliff base water levels in the infragravity band indicates that peak cliff base water levels coincide with maximum downward cliff top translation. Phase differences sometimes diverge from 180° approximately linearly with frequency, with differences as large as 45° at 0.08 Hz (Figure 4e). These phase differences may be caused by the approximately 1 s travel time between the pressure gauge and the cliff base, and by synchronization errors between the pressure gauge and seismometer. At low tide (Figure 4a), when ocean waves did not reach the cliff base, power levels of vertical ground motions at the cliff top decreased to approximately inland levels at incident wave frequencies and higher, and only infragravity-band motions were noticeably locally forced by ocean waves.

[18] The five weeks of observations (Figures 5a and 6) consistently show the features illustrated with the case example (Figure 4). Double-frequency vertical ground motions always are dominated by nonlocal sources, with approximately equal (and highly correlated, $r^2 = 0.96$) spectral levels at the coastal cliff and inland site (Figure 6c). Double-frequency cliff top ground motions and cliff base water levels are never coherent (Figure 5a). In contrast, cliff top infragravity ground motions are always dominated

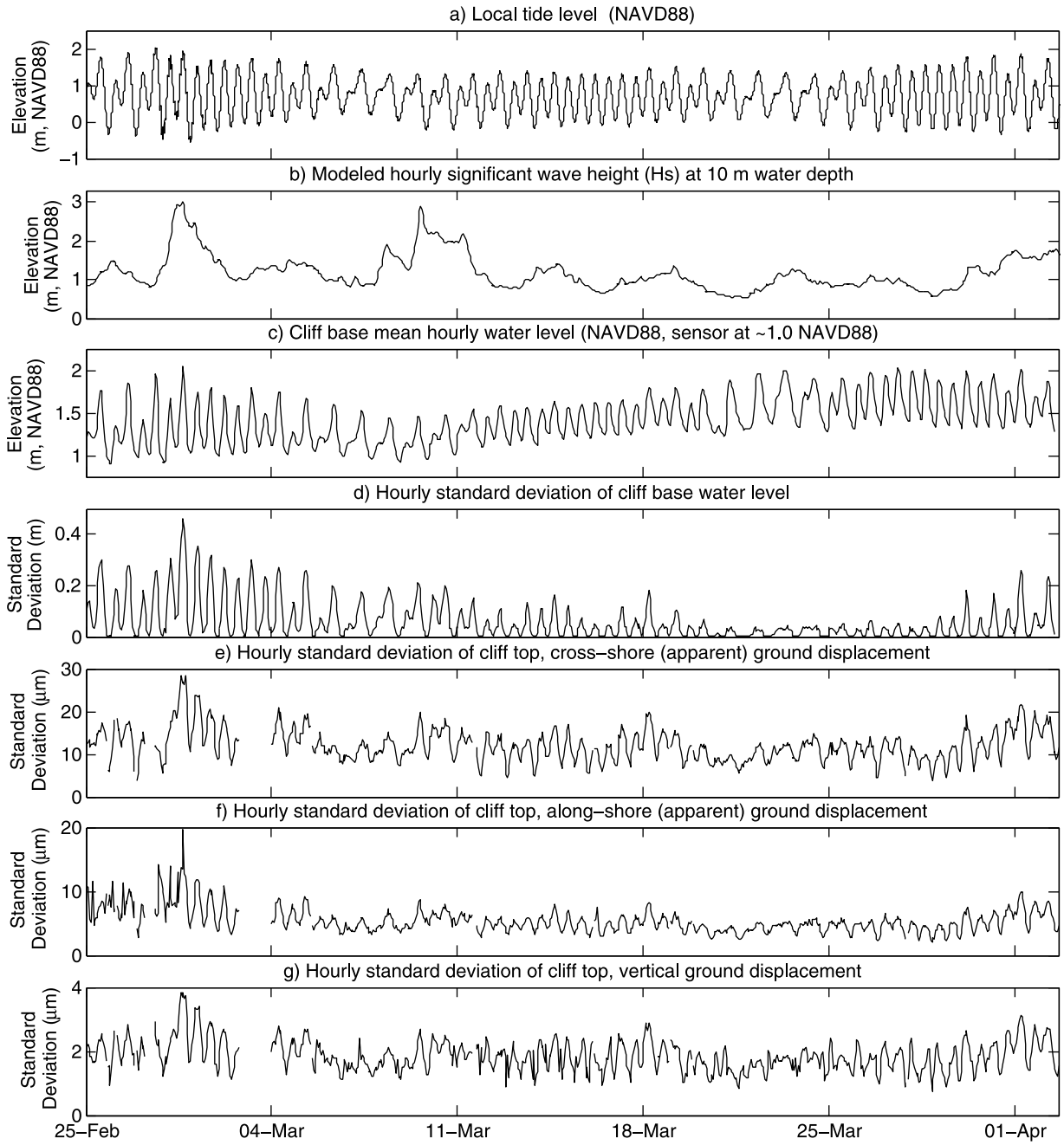

Figure 2. (a) Observed vertical local tide level (NAVD 88), (b) modeled hourly significant wave height (Hs) in 10 m water depth seaward of the study cliff, (c) mean hourly water level (NAVD88, sensor at ~1.0 NAVD88) at the cliff base, (d) hourly standard deviation of water level at the cliff base, and band passed (0.006–1 Hz) hourly standard deviation of (e) cross-shore, (f) along-shore, and (g) vertical (apparent) ground displacement versus time. Note vertical scales differ. Correlations (r^2) of cross-shore, along-shore, and vertical (apparent) ground displacement standard deviations with cliff base water level standard deviation are 0.59, 0.59, and 0.54, respectively.

by local sources, with spectral levels above inland sites (Figure 6e). When the cliff base sensor is submerged at high tide, coherence with cliff base water level fluctuations is high (Figure 5a). Single-frequency motions are locally forced at high tide (when cliff top and cliff base are coherent; Figure 5a), and remotely forced at low tide (when cliff top and inland power levels are similar; Figure 6d).

[19] Horizontal (apparent) ground displacement observed at the cliff edge are elevated above inland levels at all frequencies, including double and shaking frequencies (Figure 7). Time series of mean power averaged over the double-frequency band (a nonlocal transient ground motion) is consistently about four times larger at the cliff site than inland. The relatively large cross-shore signal (Figure 2) may

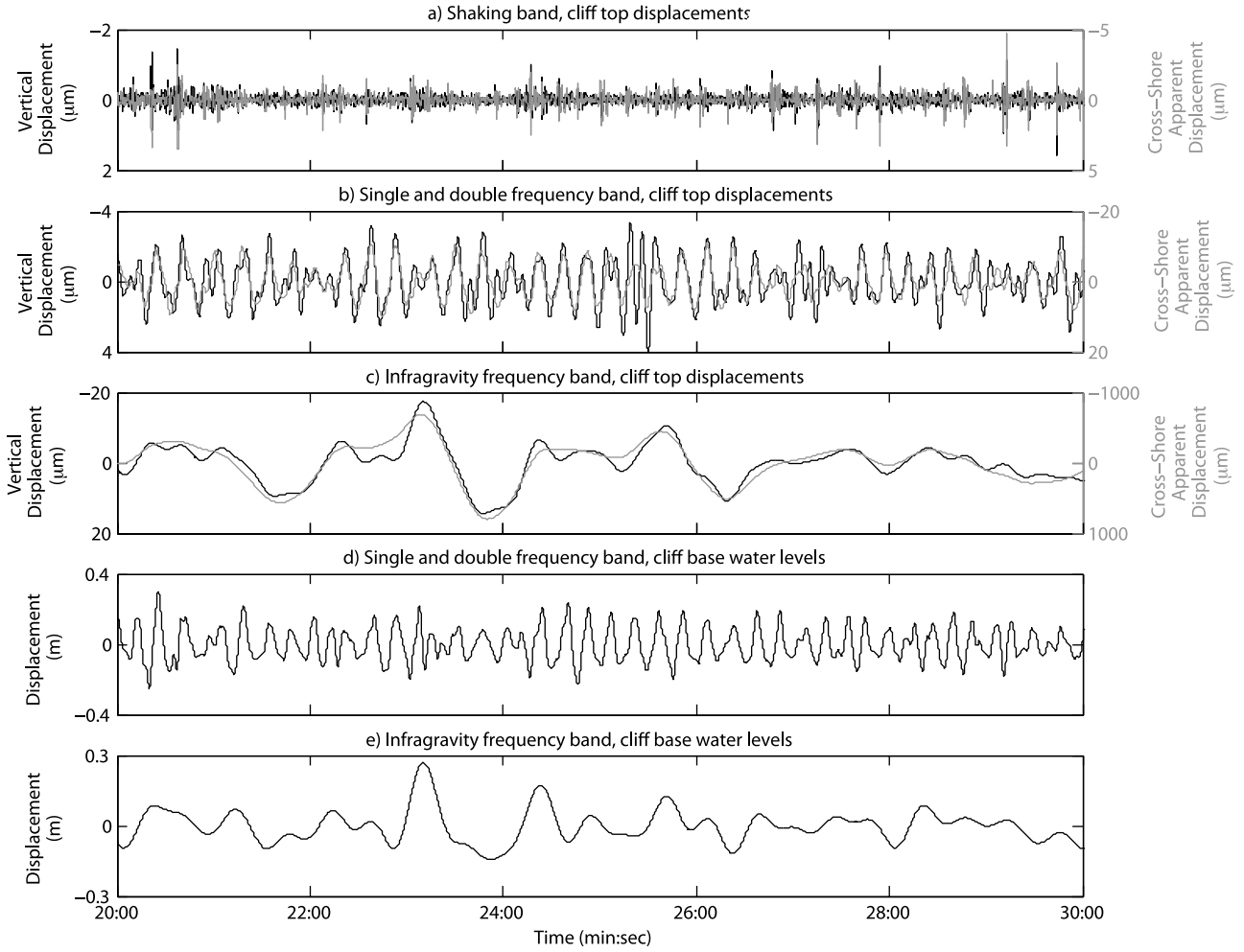

Figure 3. During high tide, vertical (black curve, left vertical axes) and (apparent) cross-shore (gray curve, right vertical axes) ground displacement versus time in the (a) shaking (>0.3 Hz), (b) single- and double (f-2f)-frequency microseism (0.05–0.30 Hz), and (c) infragravity (0.006–0.05 Hz) frequency bands. Cliff base water elevations in (d) single- and double-frequency and (e) infragravity frequency bands. Time is relative to 06:00 31 March 2010 UTC (tide level ~1.7 m NAVD88, 10 m depth Hs = 1.1 m). Note: the vertical scales differ between panels and axes.

result from ground tilt, topographic amplification [*Ashford and Sitar*, 1997; *Ashford et al.*, 1997], internal cliff structure, and the unbounded free cliff face. Ground tilt is likely a significant part of the horizontal signal at infragravity frequencies. At high tide, the phase between cliff top (apparent) horizontal displacement and cliff base water elevation indicates that horizontal motion is seaward during wave approach and landward as waves recede, consistent with previous studies [*Adams et al.*, 2005].

6. Discussion

6.1. General Observations

[20] Observations of high-frequency shaking and sea swell-induced sway are consistent with previous studies [*Adams et al.*, 2002, 2005; *Pentney*, 2010; *Lim et al.*, 2011]. Our results also confirm the local generation of low-frequency ground motions driven by ocean infragravity waves. At the studied cliff, high-frequency cliff shaking appears to be generated by direct wave-cliff interaction, while low-frequency cliff sway is generated by water level changes in the near shore. These results demonstrate a link between ocean infragravity waves at the coast and local cliff motion at Earth "hum" frequencies, however it is unknown if these motions couple significantly into propagating Earth "hum" seismic waves.

[21] Cliff motion was tidally modulated with relatively more cliff motion during elevated tidal levels. This is consistent with observations at a cliff site with similar shore platform characteristics [*Adams et al.*, 2005], but differs from sites with dissimilar platforms [*Pentney*, 2010; *Lim et al.*, 2011], suggesting that platform elevation and geometry influence ocean energy delivery to the cliffs.

6.2. Coastal Loading – Flexing

[22] Cliff sway magnitudes decreased with tide levels, suggesting the cross-shore location of gravitational load influences the magnitude of cliff top ground motion and

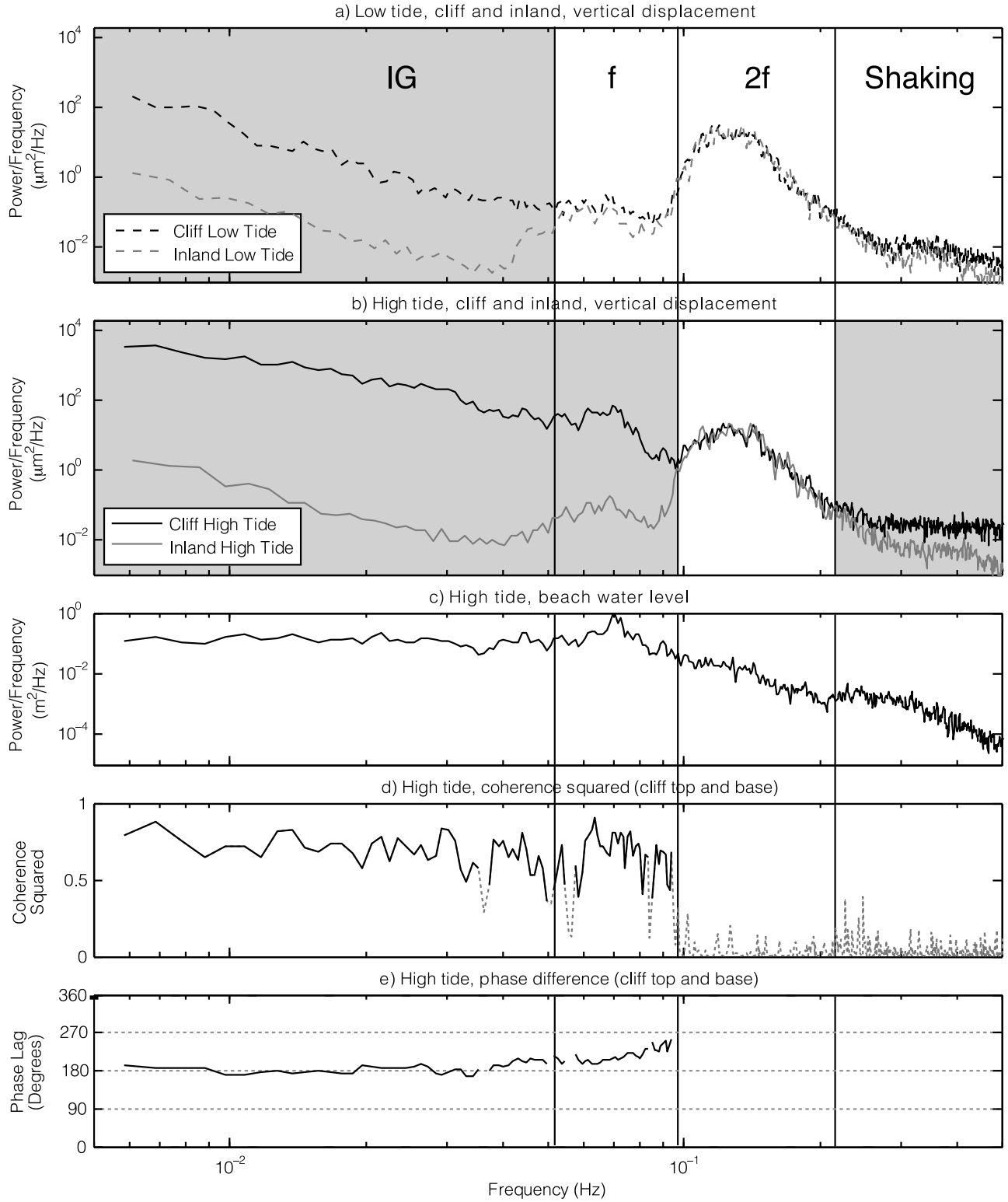

Figure 4. (a) Low-tide and (b) high-tide vertical displacement spectra at the cliff top and inland sites (see legend), (c) high-tide beach water level spectrum, (d) high-tide squared coherence (95% significance level = 0.35), and (e) phase difference between cliff base water level and cliff top vertical displacement (sign reversed). The vertical lines delineate the infragravity (*IG*), single-frequency (*f*), double-frequency (2*f*), and shaking frequency bands. Shaded (unshaded) regions include locally (remotely) forced ground motions. High and low tide times are 06:00 and 11:00 31 March 2010 UTC, tidal elevations are +1.7 m and −0.3 m, and 10 m Hs are 1.4 m and 1.1 m, respectively.

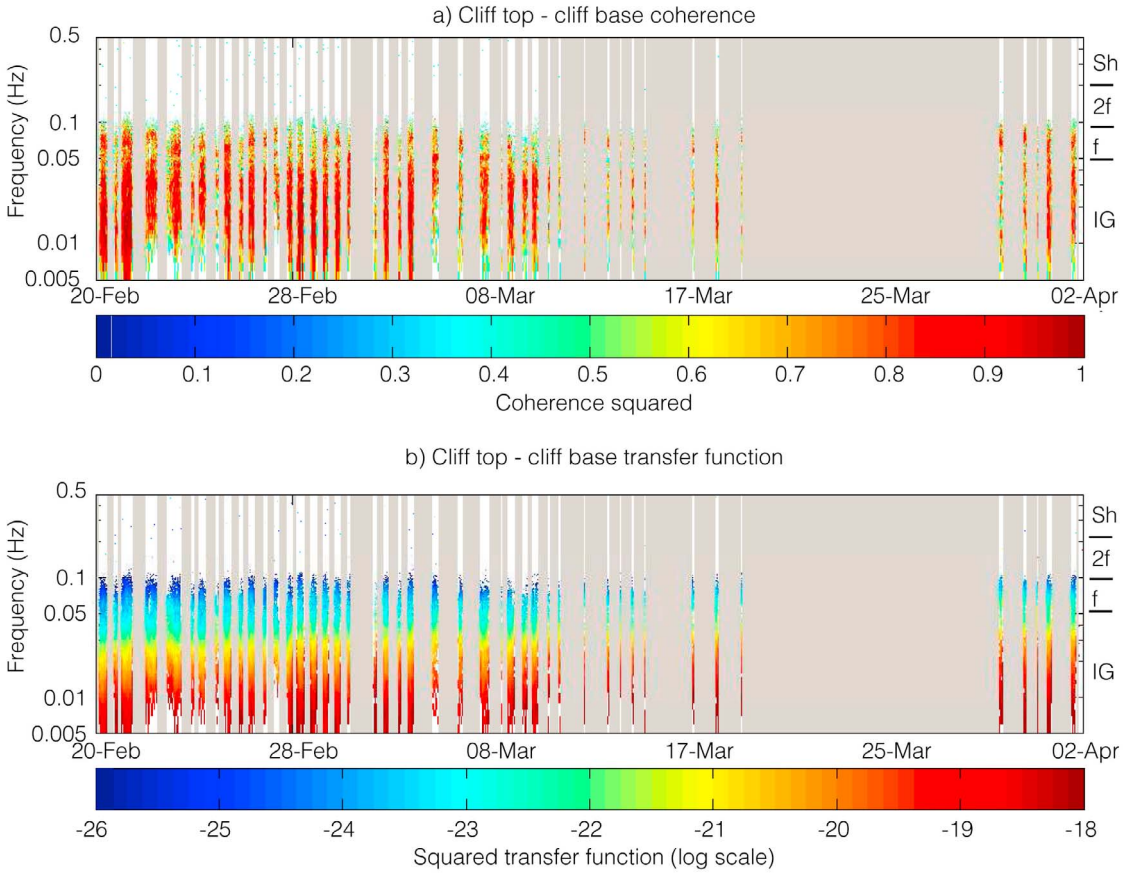

Figure 5. Time series of hourly squared (a) coherence and (b) transfer function (e.g., ratio of cliff top vertical ground motion spectra to cliff base water level spectra). In both panels, gray indicates hours with minimal cliff base wave action (hourly standard deviation less than 0.1 m), and white indicates frequencies with low coherence between cliff top and cliff base (values below 95% significance level).

transmission of ocean energy to the cliffs. The sway signal occurs continuously as individual ocean waves load and unload the shore platform and consists of downward and seaward translation and seaward tilt (Figure 8) during wave loading, and vice versa during wave unloading. The observed cliff sway signal is generally similar to other observations of coastal loading and/or tilt related to ocean tides [*Farrell*, 1972; *Agnew*, 1997] and tsunamis [*Yuan et al.*, 2005; *Nawa et al.*, 2007], and low-frequency seafloor deformation [*Webb and Crawford*, 1999, 2010].

[23] Ocean-related cliff motion decreases with distance from the cliff edge [*Adams et al.*, 2005; *Pentney*, 2010] and only far-field ocean-related "noise" (single-, double-frequency microseisms, and Earth hum frequencies) was recorded at inland site CPE. The horizontal decay of cliff motion is thought to cause cliff weakening through strain-related fatigue processes [*Adams et al.*, 2005]. The relatively large magnitude of low-frequency vertical cliff motion suggests vertical (or potentially shear) strain could be a significant source of unrecognized coastal flexing, strain, and cliff weakening. The horizontal components are affected by ground tilt, and additional research is necessary to determine the significance of cliff fatigue from long period strain.

[24] During high tide, cross-shore cliff displacement and cliff base water levels are coherent over a wide range of frequencies. The squared cliff transfer function, the ratio of cliff top ground motion spectra to cliff base water fluctuation spectra, increases at low frequency (Figure 5b). The frequency dependence of the transfer function could be caused by differences in the relationship between wave height and total gravitational load (wavelength probably also affects loading), local site effects [*Pedersen et al.*, 1994], natural cliff period excitation, or topographic seismic wave amplification [*Ashford and Sitar*, 1997; *Ashford et al.*, 1997; *Bouckovalas and Papadimitriou*, 2005]. More research is needed to assess generation and transmission of these ocean-driven ground motions.

7. Summary

[25] Ocean-wave-generated ground motions were observed at the edge of a southern California coastal cliff. At high tide, sea swell waves impacting the cliff caused high-frequency shaking. Sea swell and infragravity wave runup over the shore platform caused continuous cliff top swaying that is coherent with cliff base water levels. At low tide, when ocean waves did not reach the cliff base, power levels of vertical ground motions at the cliff top decreased to approximately inland

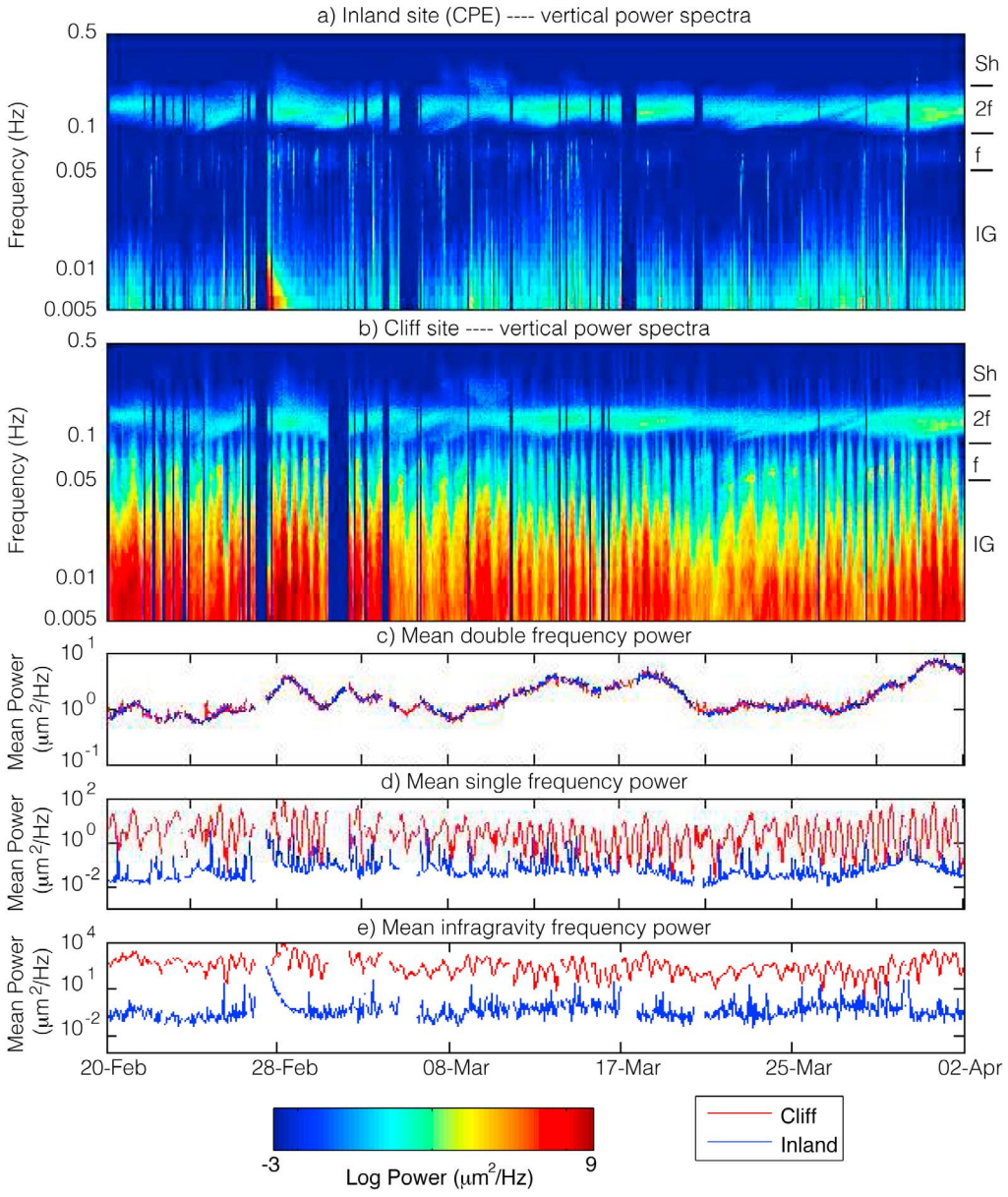

Figure 6. Vertical displacement power (see color scale) versus log frequency and time for (a) 10 km inland (Camp Elliot, CPE) and (b) cliff site. Band-integrated power versus time at inland (blue curves) and cliff (red curves) in the (c) double-frequency band, 0.10–0.30 Hz, $r^2 = 0.96$, (d) single-frequency band, 0.05–0.10 Hz, r^2 is not significant, and (e) infragravity frequency band, 0.006–0.05 Hz, r^2 is not significant. Significant earthquakes have been removed.

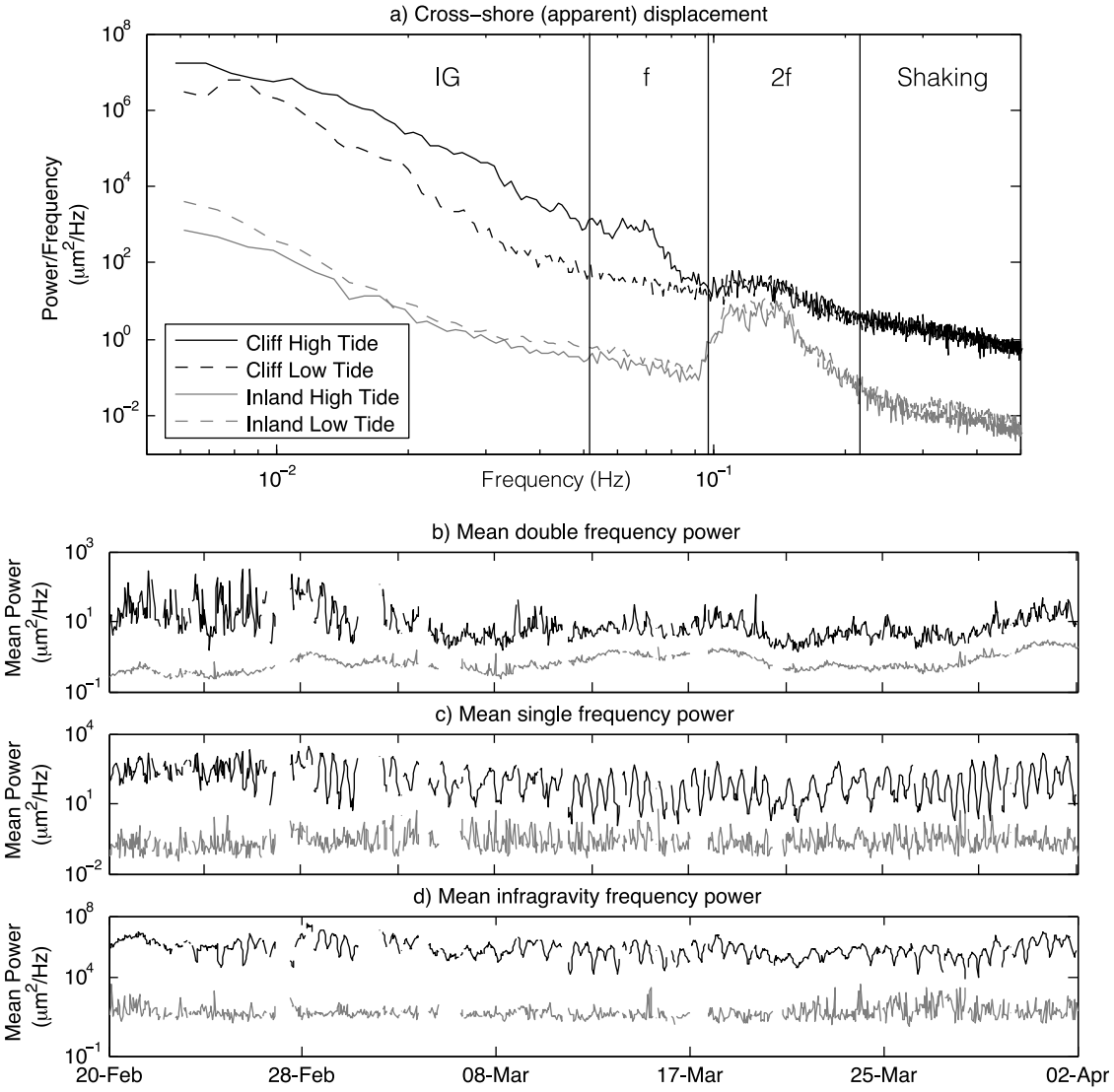

Figure 7. Horizontal (cross-shore) apparent displacement (a) spectra at high and low tide, at the cliff top and 10 km inland (see legend). Band-integrated power versus time at inland (gray curves) and cliff (black curves) in the (b) double-frequency band, 0.10–0.30 Hz, $r^2 = 0.63$. In the (c) single frequency band, 0.05–0.10 Hz, and (d) the infragravity frequency band, 0.006–0.05 Hz, r^2 is not significant. Earthquakes have been removed.

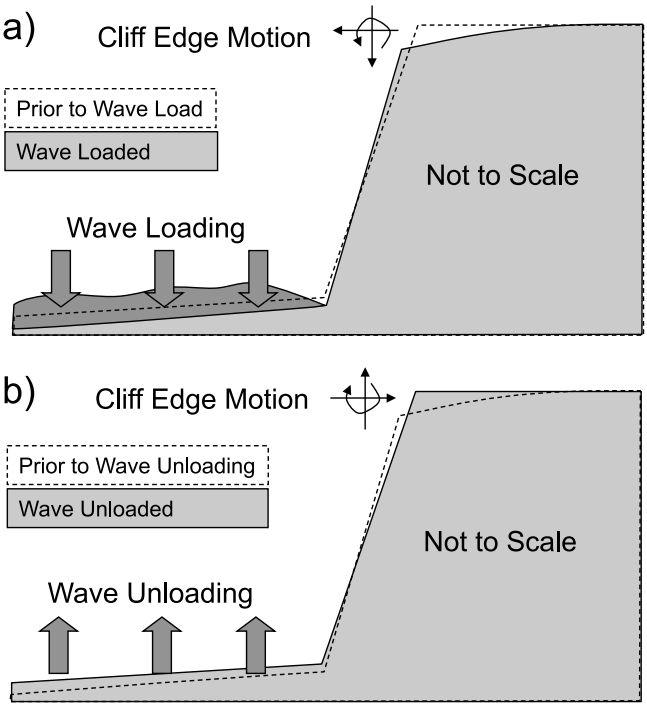

Figure 8. Cliff top edge sway motion during wave platform (a) loading, (b) unloading, and associated hypothetical changes of the shore/cliff profile.

levels at incident wave frequencies and higher, and only infragravity-band motions (0.006–0.05 Hz) were noticeably forced by local ocean waves. At all tide stages, spectra levels of vertical motions at "double frequencies" (0.1–0.3 Hz) were nearly identical at the cliff top and inland sites, consistent with a common (distant or spatially distributed) source.

[26] **Acknowledgments.** Wave data collection was sponsored by the California Department of Boating and Waterways, and the U.S. Army Corps of Engineers, as part of the Coastal Data Information Program (CDIP). A.P.Y. received Post-Doctoral Scholar support from the California Department of Boating and Waterways Oceanography Program. The California Energy Commission PIER program provided funding for this research. Portions of this work were conducted in collaboration with SPAWAR Systems Center Pacific under grant SI-1703 from the Strategic Environmental Research and Development Program (SERDP). We thank the Del Mar Beach Club, the Solana Beach Lifeguards, and the Jacobs family for their assistance.

References

Adams, P. N., R. S. Anderson, and J. Revenaugh (2002), Microseismic measurement of wave-energy delivery to a rocky coast, *Geology*, *30*(10), 895–898, doi:10.1130/0091-7613(2002)030<0895:MMOWED>2.0.CO;2.

Adams, P. N., C. D. Storlazzi, and R. S. Anderson (2005), Nearshore wave-induced cyclical flexing of sea cliffs, *J. Geophys. Res.*, *110*, F02002, doi:10.1029/2004JF000217.

Agnew, D. C. (1997), NLOADF: A program for computing ocean-tide loading, *J. Geophys. Res.*, *102*(B3), 5109–5110, doi:10.1029/96JB03458.

Agnew, D. C., and J. Berger (1978), Vertical seismic noise at very low frequencies, *J. Geophys. Res.*, *83*(B11), 5420–5424, doi:10.1029/JB083iB11p05420.

Amitrano, D., J. R. Grasso, and G. Senfaute (2005), Seismic precursory patterns before a cliff collapse and critical point phenomena, *Geophys. Res. Lett.*, *32*, L08314, doi:10.1029/2004GL022270.

Ashford, S. A., and N. Sitar (1997), Analysis of topographic amplification of inclined shear waves in a steep coastal bluff, *Bull. Seismol. Soc. Am.*, *87*(3), 692–700.

Ashford, S. A., N. Sitar, J. Lysmer, and N. Deng (1997), Topographic effects on the seismic response of steep slopes, *Bull. Seismol. Soc. Am.*, *87*(3), 701–709.

Bouckovalas, G. D., and A. G. Papadimitriou (2005), Numerical evaluation of slope topography effects on seismic ground motion, *Soil Dyn. Earthquake Eng.*, *25*, 547–558, doi:10.1016/j.soildyn.2004.11.008.

Bromirski, P. D. (2001), Vibrations from the "perfect storm," *Geochem. Geophys. Geosyst.*, *2*(7), 1030, doi:10.1029/2000GC000119.

Bromirski, P. D., R. E. Flick, and N. Graham (1999), Ocean wave height determined from inland seismometer data: Implications for investigating wave climate changes in the NE Pacific, *J. Geophys. Res.*, *104*(C9), 20,753–20,766, doi:10.1029/1999JC900156.

Bromirski, P. D., O. V. Sergienko, and D. R. MacAyeal (2010), Transoceanic infragravity waves impacting Antarctic ice shelves, *Geophys. Res. Lett.*, *37*, L02502, doi:10.1029/2009GL041488.

Cathles, L. M., E. A. Okal, and D. R. MacAyeal (2009), Seismic observations of sea swell on the floating Ross Ice Shelf, Antarctica, *J. Geophys. Res.*, *114*, F02015, doi:10.1029/2007JF000934.

Crawford, W. C., and S. C. Webb (2000), Identifying and removing tilt noise from low-frequency (<0.1 Hz) seafloor vertical seismic data, *Bull. Seismol. Soc. Am.*, *90*(4), 952–963, doi:10.1785/0119990121.

Crawford, W. C., S. C. Webb, and J. A. Hildebrand (1991), Seafloor compliance observed by long-period pressure and displacement measurements, *J. Geophys. Res.*, *96*(B10), 16,151–16,160, doi:10.1029/91JB01577.

Dolenc, D., B. Romanowicz, D. Stakes, P. McGill, and D. Neuhauser (2005), Observations of infragravity waves at the Monterey Ocean bottom broadband station (MOBB), *Geochem. Geophys. Geosyst.*, *6*, Q09002, doi:10.1029/2005GC000988.

Dolenc, D., B. Romanowicz, R. Uhrhammer, P. McGill, D. Neuhauser, and D. Stakes (2007), Identifying and removing noise from the Monterey ocean bottom broadband seismic station (MOBB) data, *Geochem. Geophys. Geosyst.*, *8*, Q02005, doi:10.1029/2006GC001403.

Dolenc, D., B. Romanowicz, P. McGill, and W. Wilcock (2008), Observations of infragravity waves at the ocean-bottom broadband seismic stations Endeavour (KEBB) and Explorer (KXBB), *Geochem. Geophys. Geosyst.*, *9*, Q05007, doi:10.1029/2008GC001942.

Farrell, W. E. (1972), Deformation of the Earth by surface loads, *Rev. Geophys.*, *10*(3), 761–797, doi:10.1029/RG010i003p00761.

Graizer, V. (2006), Tilts in strong ground motion, *Bull. Seismol. Soc. Am.*, *96*(6), 2090–2102, doi:10.1785/0120060065.

Haubrich, R. A., and K. McCamy (1969), Microseisms: Coastal and pelagic sources, *Rev. Geophys.*, *7*(3), 539–571, doi:10.1029/RG007i003p00539.

Haubrich, R. A., W. H. Munk, and F. E. Snodgrass (1963), Comparative spectra of microseisms and swell, *Bull. Seismol. Soc. Am.*, *53*(1), 27–37.

Jenkins, G. M., and D. G. Watts (1968), *Spectral Analysis and Its Applications*, Holden-Day, San Francisco, Calif.

Kennedy, M. P. (1975), Geology of the San Diego metropolitan area, western area, *Bull. 200*, Calif. Div. Mines Geol., Sacramento, Calif.

Kibblewhite, A. C., and C. Y. Wu (1991), The theoretical description of wave-wave interactions as a noise source in the ocean, *J. Acoust. Soc. Am.*, *89*(5), 2241–2252, doi:10.1121/1.400970.

Lim, M., N. J. Rosser, D. N. Petley, and M. Keen (2011), Quantifying the controls and influence of tide and wave impacts on coastal rock cliff erosion, *J. Coastal Res.*, *27*(1), 46–56, doi:10.2112/JCOASTRES-D-09-00061.1.

Longuet-Higgins, M. S. (1950), A theory of the origin of microseisms, *Philos. Trans. R. Soc. London*, *243*(857), 1–35, doi:10.1098/rsta.1950.0012.

MacAyeal, D. R., et al. (2006), Transoceanic wave propagation links iceberg calving margins of Antarctica with storms in tropics and Northern Hemisphere, *Geophys. Res. Lett.*, *33*, L17502, doi:10.1029/2006GL027235.

MacAyeal, D. R., E. A. Okal, R. C. Aster, and J. N. Bassis (2009), Seismic observations of glaciogenic ocean waves (micro-tsunamis) on icebergs and ice shelves, *J. Glaciol.*, *55*(190), 193–206, doi:10.3189/002214309788608679.

Nawa, K., N. Suda, K. Satake, Y. Fujii, T. Sato, K. Doi, M. Kanao, and K. Shibuya (2007), Loading and gravitational effects of the 2004 Indian Ocean tsunami at Syowa Station, Antarctica, *Bull. Seismol. Soc. Am.*, *97*(1A), S271–S278, doi:10.1785/0120050625.

O'Reilly, W. C., and R. T. Guza (1991), Comparison of spectral refraction and refraction-diffraction save models, *J. Waterw. Port Coastal Ocean Eng.*, *117*(3), 199–215, doi:10.1061/(ASCE)0733-950X(1991)117:3(199).

O'Reilly, W. C., and R. T. Guza (1993), A comparison of two spectral wave models in the southern California Bight, *Coastal Eng.*, *19*, 263–282, doi:10.1016/0378-3839(93)90032-4.

O'Reilly, W. C., and R. T. Guza (1998), Assimilating coastal wave observations in regional swell predictions. Part I: Inverse methods, *J. Phys.*

Oceanogr., *28*(4), 679–691, doi:10.1175/1520-0485(1998)028<0679:ACWOIR>2.0.CO;2.

Pawka, S. S. (1983), Island shadows in wave directional spectra, *J. Geophys. Res.*, *88*(C4), 2579–2591, doi:10.1029/JC088iC04p02579.

Pedersen, H., B. Lebrun, D. Hatzfeld, M. Campillo, and P. Y. Bard (1994), Ground-motion amplitude across ridges, *Bull. Seismol. Soc. Am.*, *84*(6), 1786–1800.

Pentney, R. (2010), Seismic measurements of wave energy delivery to a rocky coastline: Okakari Point, Auckland, New Zealand, Masters thesis, Univ. Auckland, New Zealand.

Rhie, J., and B. Romanowicz (2004), Excitation of Earth's continuous free oscillations by atmosphere-ocean-seafloor coupling, *Nature*, *431*(7008), 552–556, doi:10.1038/nature02942.

Rhie, J., and B. Romanowicz (2006), A study of the relation between ocean storms and the Earth's hum, *Geochem. Geophys. Geosyst.*, *7*, Q10004, doi:10.1029/2006GC001274.

Rodgers, P. W. (1968), Response of horizontal pendulum seismometer to Rayleigh and love waves tilt and free oscillations of Earth, *Bull. Seismol. Soc. Am.*, *58*(5), 1384–1406.

Senfaute, G., A. Duperret, and J. A. Lawrence (2009), Micro-seismic precursory cracks prior to rock-fall on coastal chalk cliffs: A case study at Mesnil-Val, Normandie, NW France, *Nat. Hazard Earth Syst. Sci.*, *9*, 1625–1641, doi:10.5194/nhess-9-1625-2009.

Tillotson, K., and P. D. Komar (1997), The wave climate of the Pacific Northwest (Oregon and Washington): A comparison of data sources, *J. Coastal Res.*, *13*(2), 440–452.

Webb, S. C. (2007), The Earth's 'hum' is driven by ocean waves over the continental shelves, *Nature*, *445*, 754–756, doi:10.1038/nature05536.

Webb, S. C., and W. C. Crawford (1999), Long-period seafloor seismology and deformation under ocean waves, *Bull. Seismol. Soc. Am.*, *89*(6), 1535–1542.

Webb, S. C., and W. C. Crawford (2010), Shallow-water broadband OBS seismology, *Bull. Seismol. Soc. Am.*, *100*(4), 1770–1778, doi:10.1785/0120090203.

Yuan, X., R. Kind, and H. A. Pedersen (2005), Seismic monitoring of the Indian Ocean tsunami, *Geophys. Res. Lett.*, *32*, L15308, doi:10.1029/2005GL023464.

P. N. Adams, Department of Geological Sciences, University of Florida, 241 Williamson Hall, PO Box 112120, Gainesville, FL 32611, USA.

R. E. Flick, R. T. Guza, W. C. O'Reilly, and A. P. Young, Integrative Oceanography Division, Scripps Institution of Oceanography, University of California San Diego, 9500 Gilman Dr., La Jolla, CA 92093-0209, USA. (adyoung@ucsd.edu)